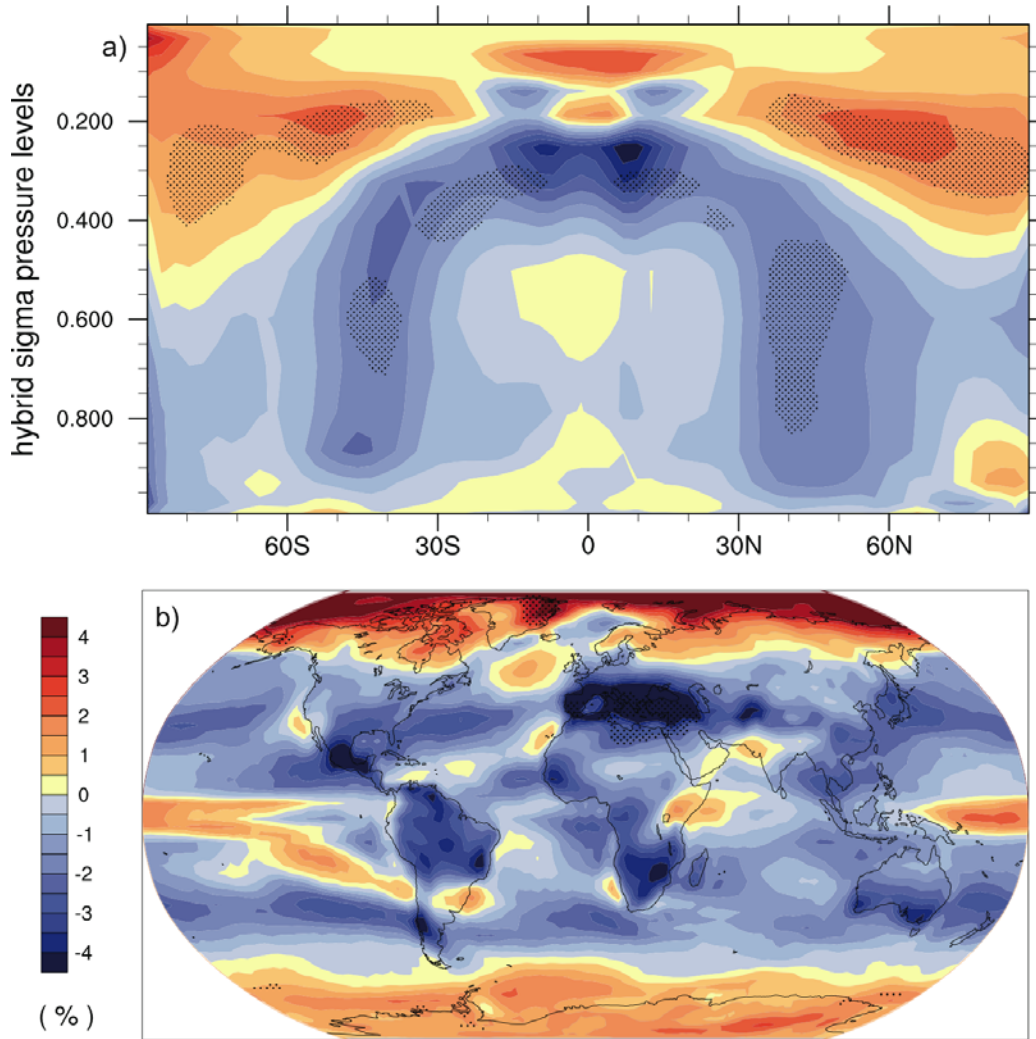


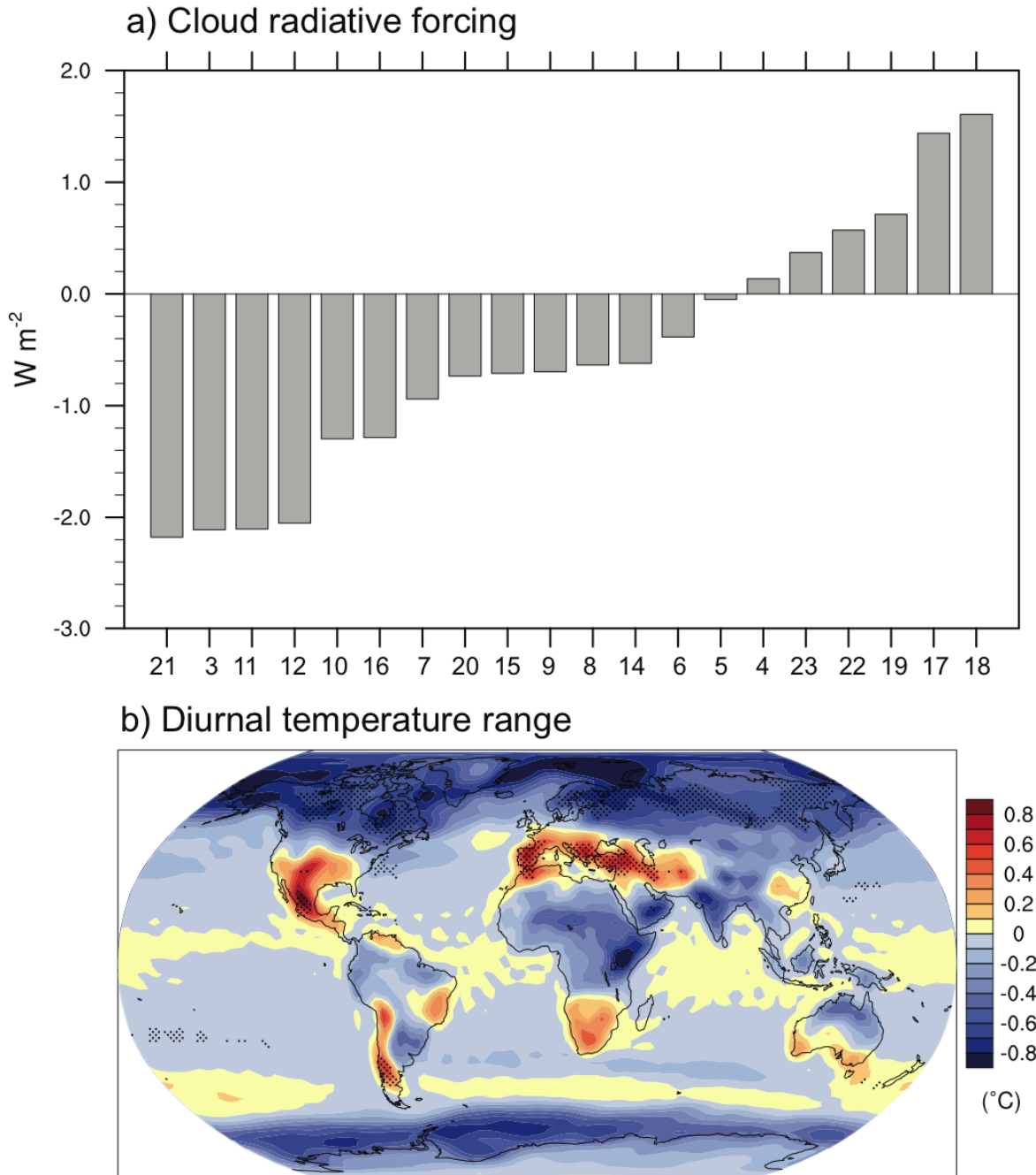
1



2  
3  
4  
5  
6  
7  
8  
9  
10  
11

**Figure 10.3.7.** Multi model mean changes in a) zonal mean cloud fraction (in %), shown as a cross section through the atmosphere, and b) total cloud area fraction (in percentage cover from all models). Changes are given as annual means for the scenarios SRES A1B, for the period 2080–2099 relative to 1980–1999. Stippling denotes areas where the magnitude of the multi-model ensemble mean exceeds the inter-model standard deviation. Results for individual models can be seen in supplementary material for this chapter.

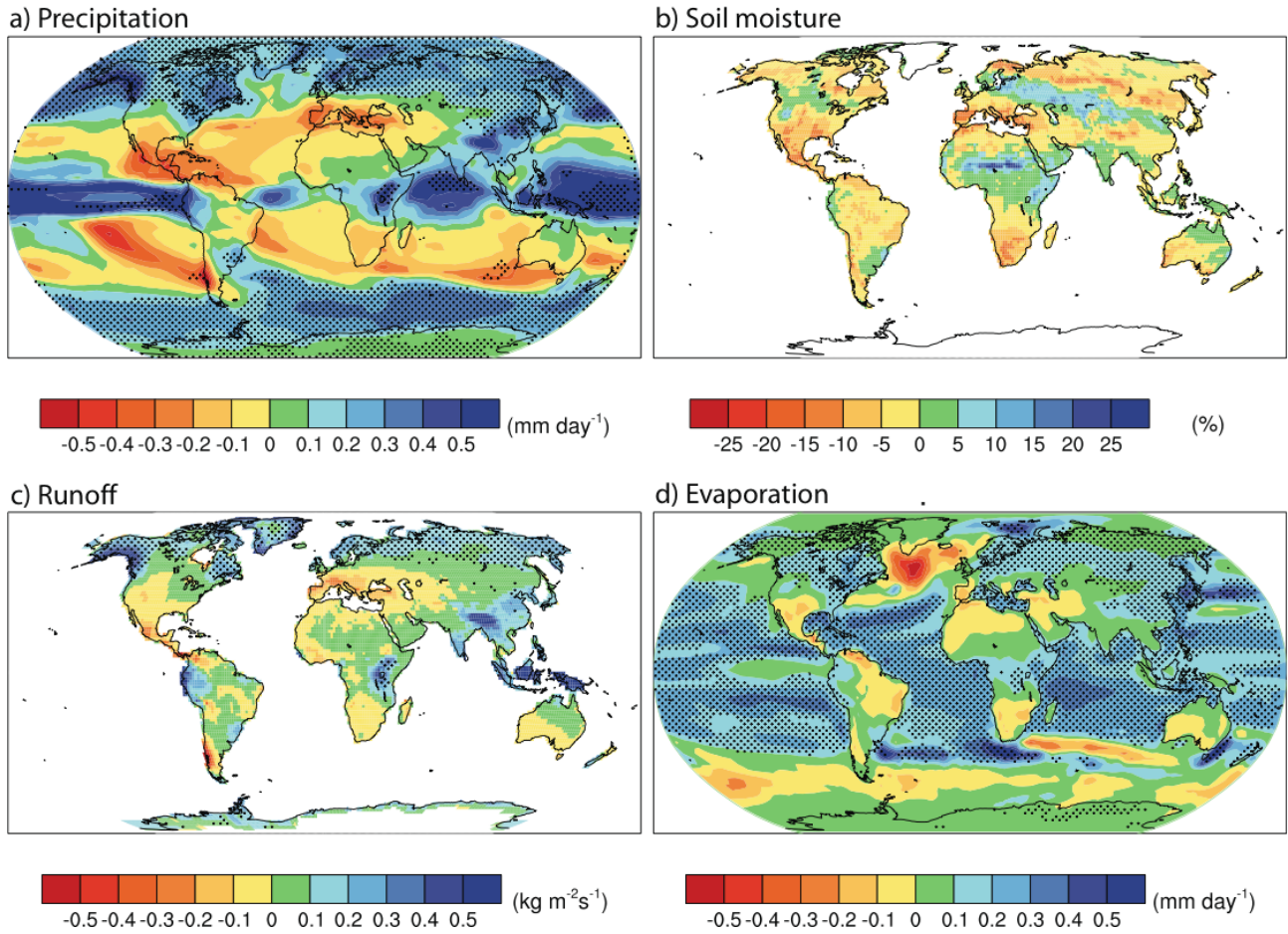
1  
2



3  
4  
5  
6  
7  
8  
9  
10  
11

**Figure 10.3.8.** Changes in a) global mean cloud radiative forcing (in  $W m^{-2}$ ) from individual models (see Chapter 8, Table 8.1 for the list of models), and b) multi-model mean diurnal temperature range ( $^{\circ}C$ ). Changes are given as annual means for the scenarios SRES A1B, for the period 2080–2099 relative to 1980–1999. Stippling denotes areas where the magnitude of the multi-model ensemble mean exceeds the inter-model standard deviation. Results for individual models can be seen in supplementary material for this chapter.

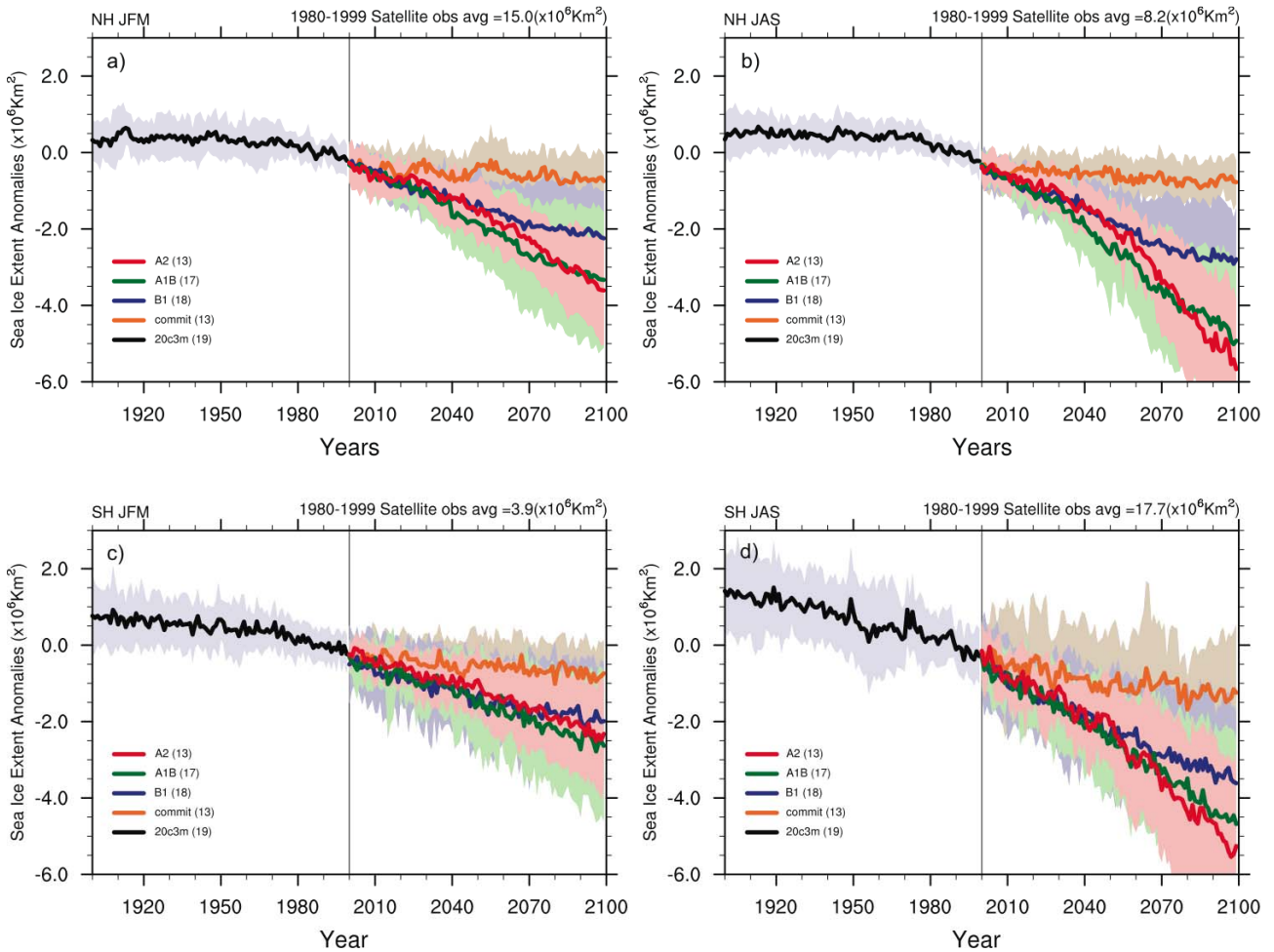
1  
2



3  
4  
5  
6  
7  
8  
9  
10  
11

**Figure 10.3.9.** Multi model mean changes in a) precipitation (mm/day), b) soil moisture content (%), c) runoff (kg/m<sup>2</sup>s), and d) evaporation (mm/day). Note that “soil moisture content” is the best estimate of this quantity supplied by each model, but calculations vary across models. Changes are given as annual means for the scenarios SRES A1B, for the period 2080–2099 relative to 1980–1999. Stippling denotes areas where the magnitude of the multi-model ensemble mean exceeds the inter-model standard deviation. Results for individual models can be seen in supplementary material for this chapter.

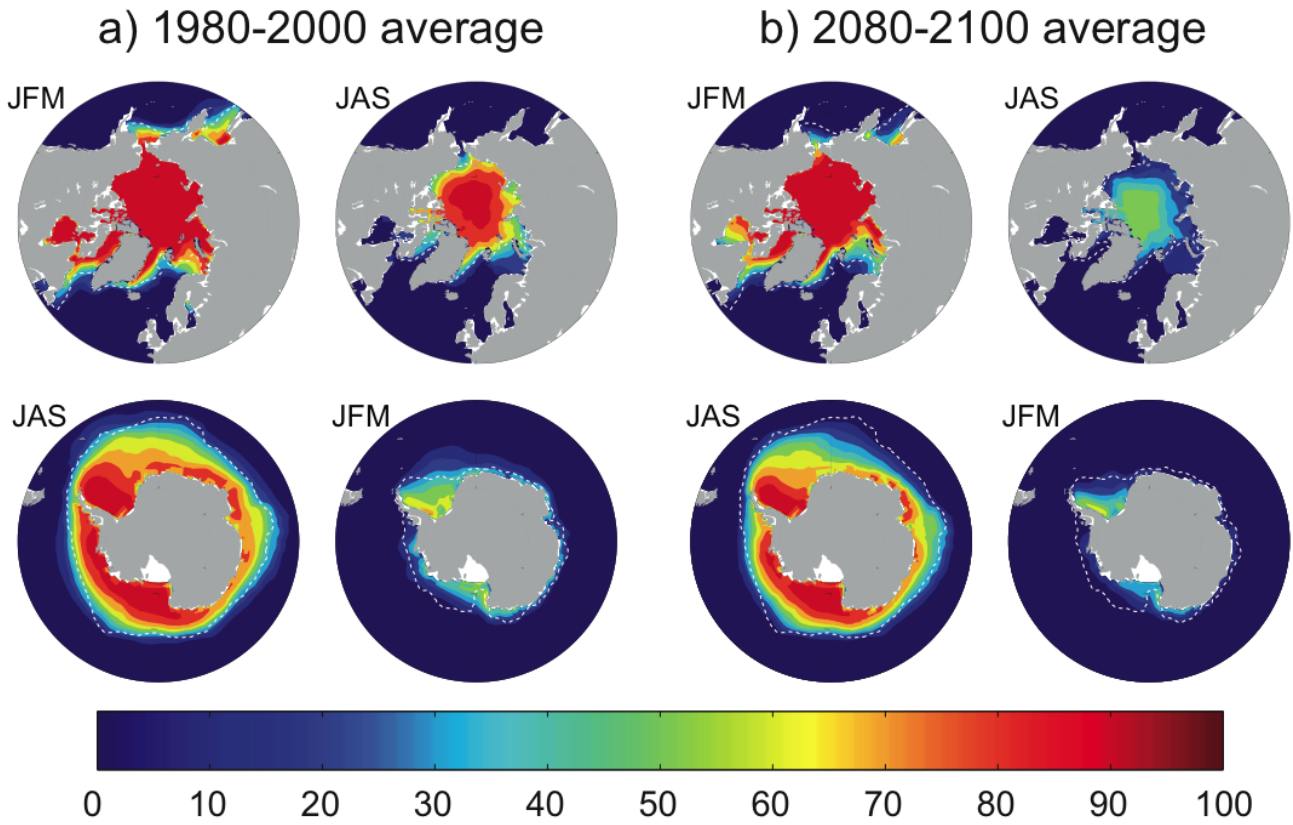
1  
2



3  
4  
5  
6  
7  
8  
9  
10  
11

**Figure 10.3.10.** Multi model simulated anomalies in sea ice extent for the 20th century, the SRES A2, A1B and B1 as well as the commitment scenario, for (panel a) Northern Hemisphere January to March (JFM), (panel b) Northern Hemisphere July to September (JAS). Panels c and d are as for a and b but for the Southern Hemisphere. The solid lines show the multi model mean, shaded areas denote plus minus one standard deviation. Sea ice extent is defined as the total area where sea ice concentration exceeds 15%. Anomalies are shown relative to the period 1980–2000. The number of models is given in the legend and is different for each scenario.

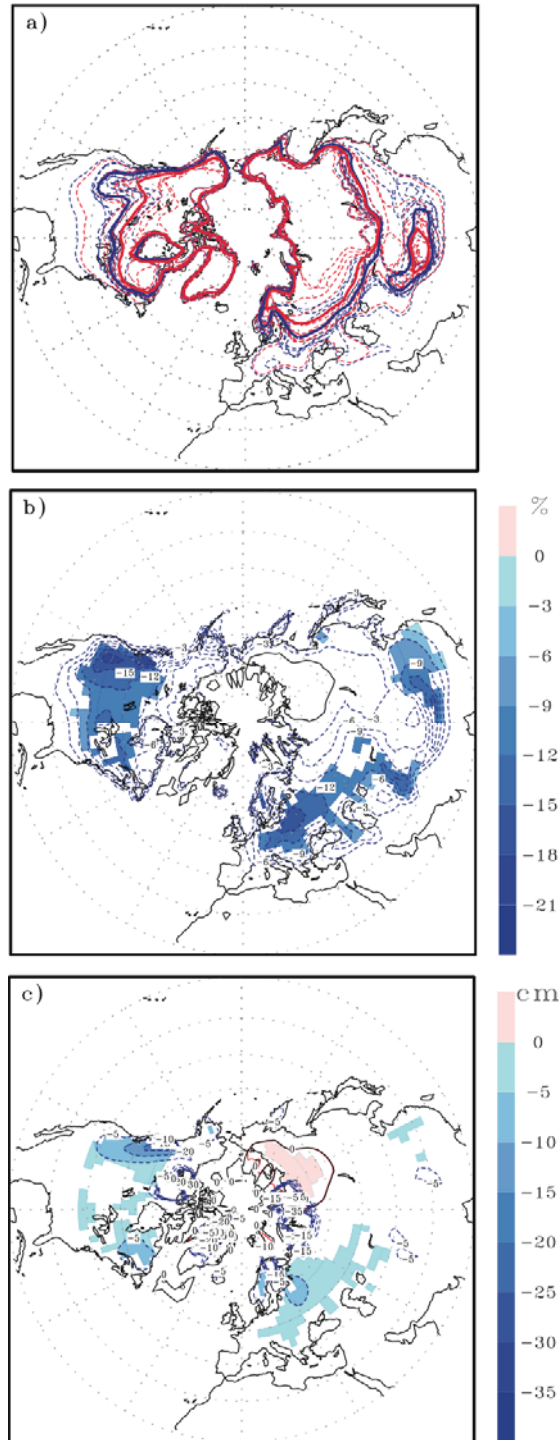
1  
2



3  
4  
5  
6  
7  
8  
9  
10

**Figure 10.3.11.** Multi-model mean sea ice concentration (in %) for January to March (JFM) and June to September (JAS), Arctic (top) and Antarctic (bottom) for the periods a) 1980–2000 and b) 2080–2100 for the scenario SRES A1B. The dashed white line indicates the present-day 15% average sea-ice concentration limit. Modified from Flato et al. (2004).

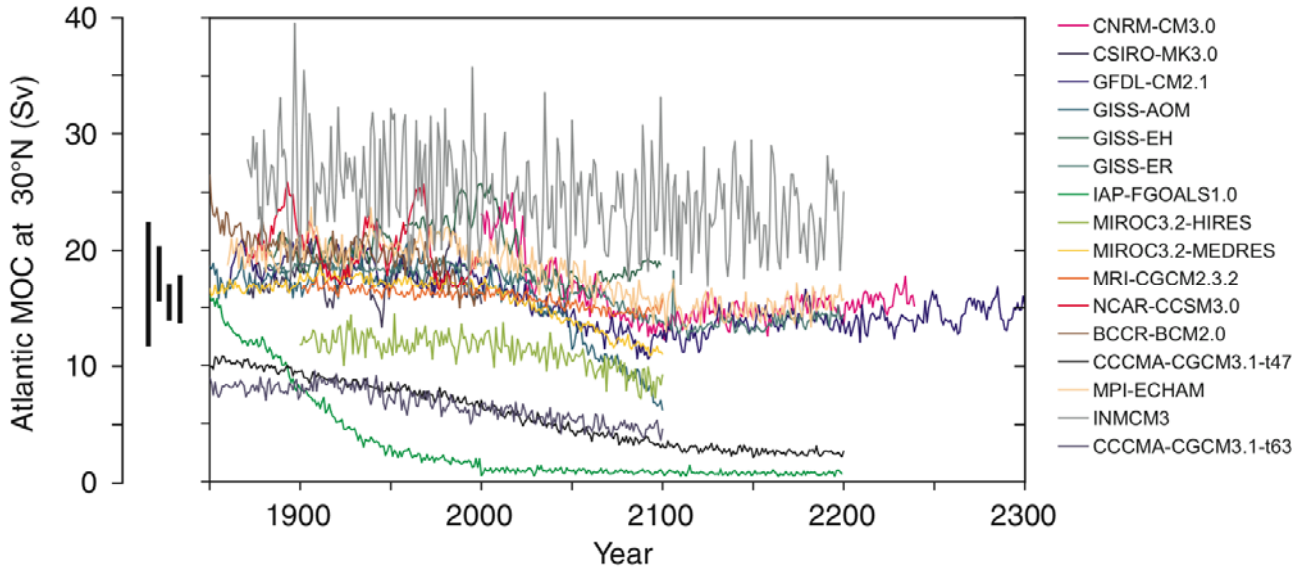
1  
2



3  
4  
5  
6  
7  
8  
9  
10  
11  
12

**Figure 10.3.12.** Multi model mean snow cover and projected changes over the 21st century from 12 (a and b) and 11 (c) AOGCMs, respectively. a) Contours mark the locations where the December to February (DJF) snow area fraction exceeds 50%, blue for the period 1980–1999, and red for 2080–2099, dashed for the individual models and solid for the multi model mean. b) Projected multi model mean change in snow area fraction over the period 2080–2099, relative to 1980–1999. Shading denotes regions where the ensemble mean divided by the ensemble standard deviation exceeds 1.0 (in magnitude), c) as b) but changes in snow depth (in cm).

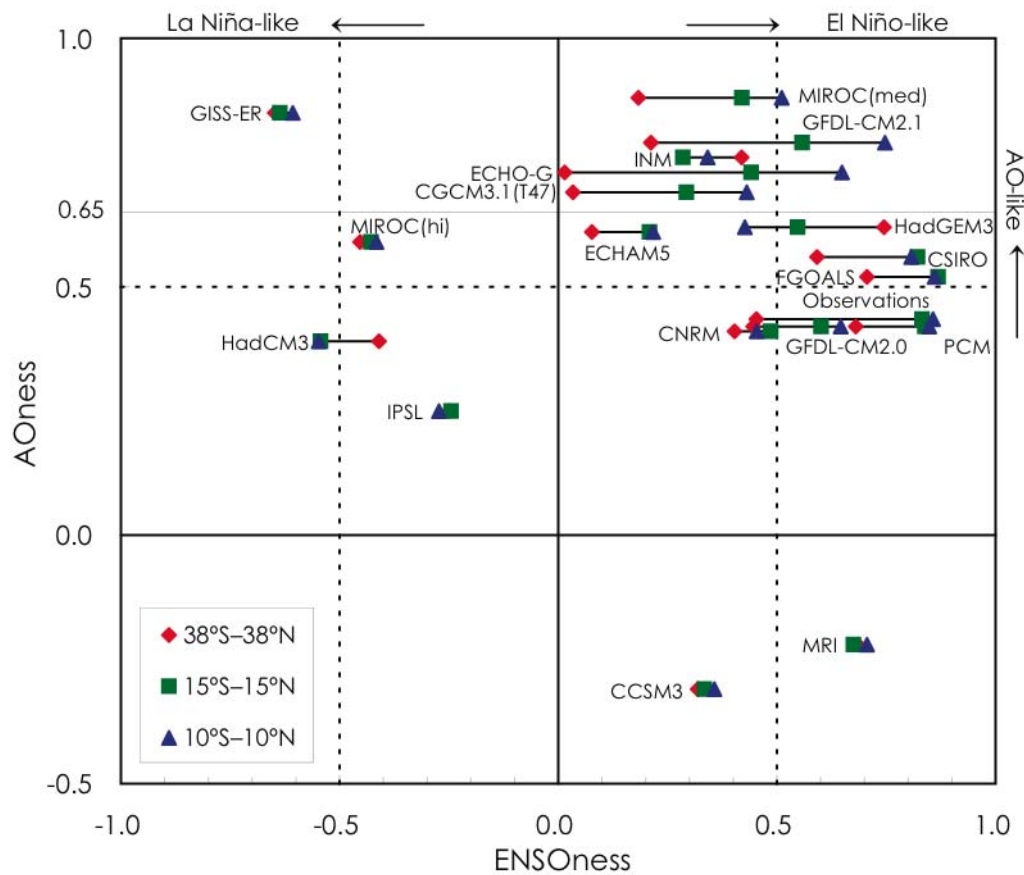
1  
2



3  
4  
5  
6  
7  
8  
9  
10  
11  
12  
13  
14  
15  
16  
17

**Figure 10.3.13.** Evolution of the Atlantic meridional overturning circulation (MOC) at 30°N in simulations with the suite of comprehensive coupled climate models from 1850 to 2100 using scenarios 20C3M for 1850 to 1999 and emissions scenario SRES A1B for 1999 to 2100. Some of the models continue the integration to year 2300 with the forcing held constant at the values of year 2100. Observationally based estimates of late 20th century MOC are given as vertical bars. Two models show a steady or rapid spin down of the MOC which is unrelated to the forcing; two others have late 20th century simulated values that are inconsistent with observational estimates. Of the model simulations consistent with the late 20th century observational estimates, no simulation shows an increase of MOC during the 21st century; reductions range from indistinguishable within the simulated natural variability to 60% relative to the 1960–1990 mean; none of the models projects an abrupt transition to an off state of the MOC. Adapted from Schmittner et al., (2005) with additions.

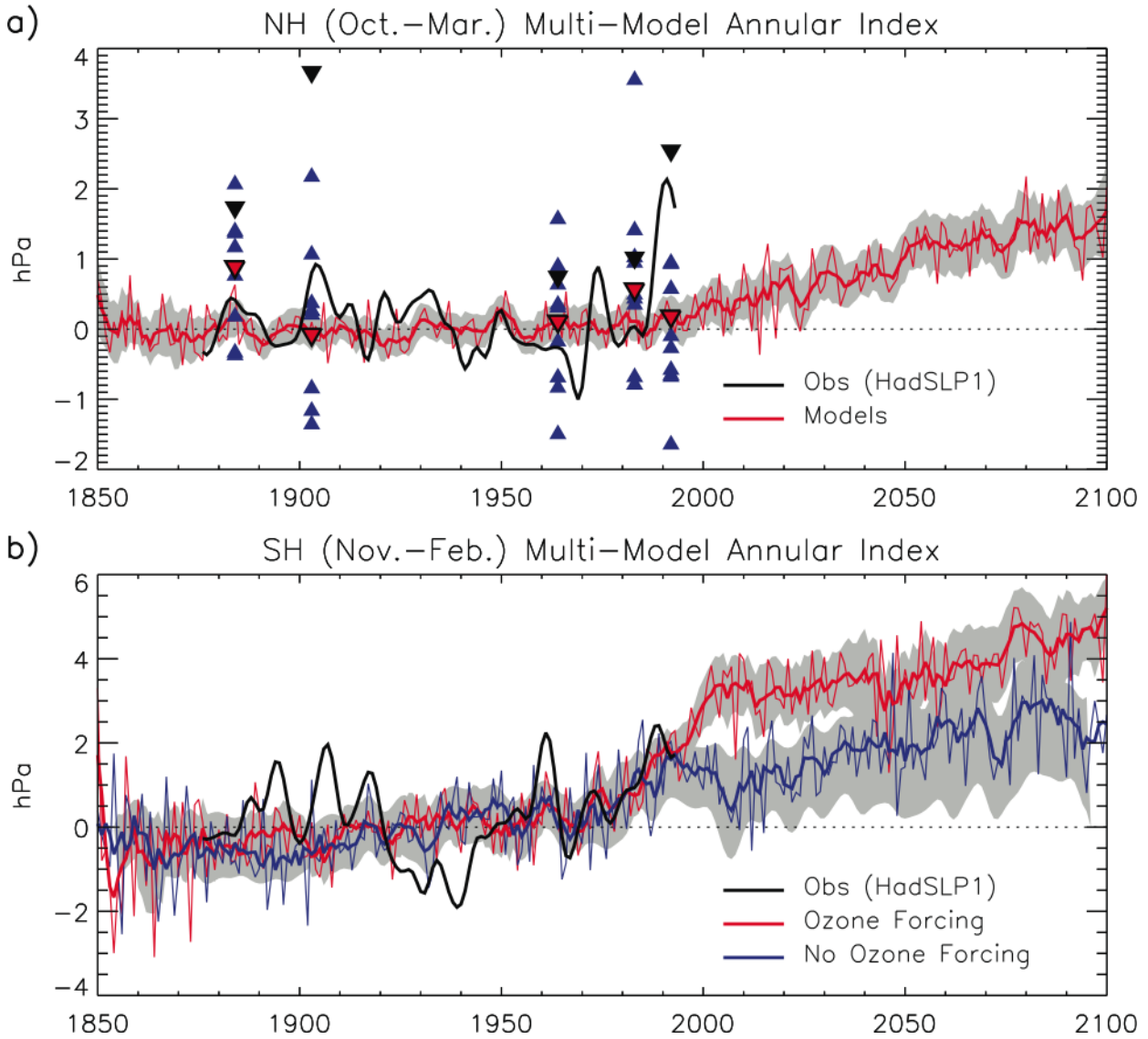
1  
2



3  
4  
5  
6  
7  
8  
9  
10  
11

**Figure 10.3.14.** Scatter plot of “ENSOness” versus “AOness” for the simulated trend patterns. “ENSOness” is expressed in terms of the anomaly pattern correlation coefficients between the linear trend of the 1% CO<sub>2</sub> experiments and the first EOF of the SST in the control experiments for three latitudinal zones with different width, i.e., 10°S–10°N, 15°S–15°N, and 38°S–38°N for longitudinal range 120°E–60°W. “AOness” is expressed in terms of the anomaly pattern correlation coefficients between the CO<sub>2</sub>-induced trend and the first EOF of the SLP north of 20°N. Modified from Yamaguchi and Noda (2006).

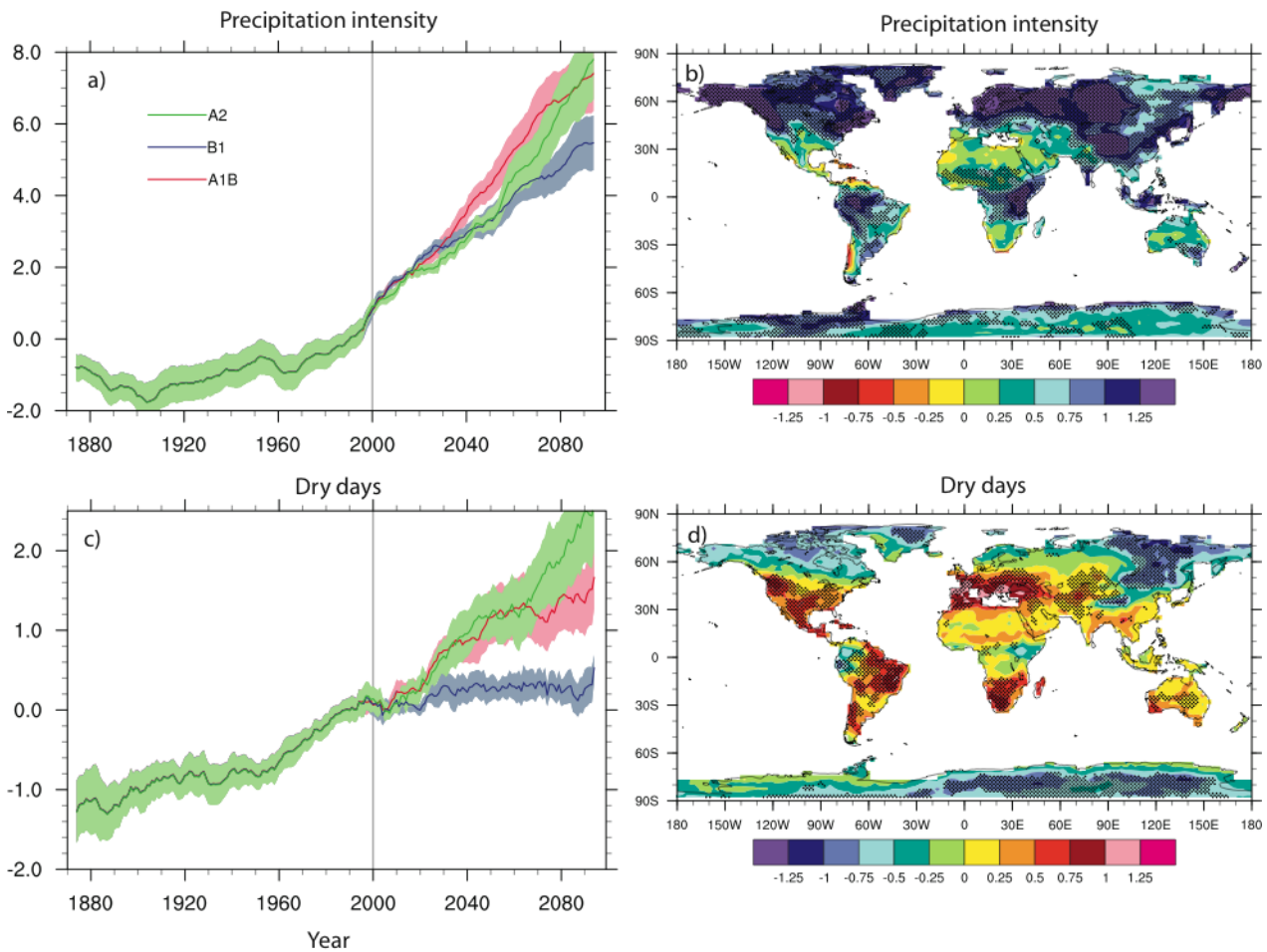
1  
2



3  
4  
5  
6  
7  
8  
9  
10  
11  
12  
13  
14

**Figure 10.3.15.** (a) Multi model mean of the regression of the leading EOF of ensemble mean Northern Hemisphere sea level pressure (NH SLP, thin red). The time series of regression coefficients has zero mean between year 1900 and 1970. The thick red line is a 10-year low-passed filtered version of the mean. The gray shading represents the inter-model spread at the 95% level and is filtered. A filtered version of the observed SLP is in black. The regression coefficient for the winter following a major tropical eruption is marked by red, blue, and black triangles, respectively, for the multi-model mean, the individual model mean, and observations. (b) as in (a) except for the Southern Hemisphere SLP for models with (red) and without (blue) ozone forcing. From Miller et al. (2006)

1  
2



3  
4  
5  
6  
7  
8  
9  
10  
11  
12  
13  
14  
15  
16  
17  
18  
19  
20

**Figure 10.3.16.** Changes in extremes based on multi-model simulations from nine global coupled climate models, adapted from Tebaldi et al. (2006). a) Globally averaged changes in precipitation intensity (defined as the annual total precipitation divided by the number of wet days) for a low (SRES B1), middle (SRES A1B), and high (SRES A2) scenario. b) Changes of spatial patterns of precipitation intensity based on simulations between two 20-year means (2080–2099 minus 1980–1999) for the A1B scenario. c) Globally averaged changes in dry days (defined as the annual maximum number of consecutive dry days). d) changes of spatial patterns of dry days based on simulations between two 20-year means (2080–2099 minus 1980–1999) for the A1B scenario. Solid lines in panels a and c are the 10-year smoothed multi-model ensemble means, the envelope indicates the ensemble mean standard deviation. Stippling in panels b and d denote areas where at least 5 of the 9 models concur in determining that the change is statistically significant. Extreme indices are calculated only over land. Extremes indices are calculated following Frich et al. (2002). Each model's timeseries has been centered around its 1980–1999 average and normalized (rescaled) by its standard deviation computed (after detrending) over the period 1960–2099, then the models were aggregated into an ensemble average, both at the global average and at the grid-box level. Thus, changes are given in units of standard deviations.